Solid Earth Discuss., 4, 203–239, 2012
www.solid-earth-discuss.net/4/203/2012/
doi:10.5194/sed-4-203-2012

Solid Earth Discussions

Possibility of titanium transportation within a mantle wedge: formation process of titanoclinohumite in Fujiwara dunite in Sanbagawa belt, Japan

S. Ishimaru[1,2] **and S. Arai**[2]

[1]Guraduate School of Science and Technology, Department of Earth and Environmental Sciences, Kumamoto University, 2-39-1 Kurokami, Kumamoto 860–8555, Japan
[2]Earth Science Course, School of Natural System, College of Science and Engineering, Kanazawa University, Kakuma, Kanazawa 920–1192, Japan

Received: 1 December 2011 – Accepted: 4 January 2012 – Published: 27 January 2012

Correspondence to: S. Ishimaru (ishimaru@sci.kumamoto-u.ac.jp)

Published by Copernicus Publications on behalf of the European Geosciences Union.

Abstract

Titinoclinohumite-bearing dunites from Fujiwara, the Sanbagawa metamorphic belt of high-pressure type, Japan, were described to examine the possibility of Ti mobility during metasomatism within the mantle wedge. The Fujiwara dunite body and surrounding high-pressure Sanbagawa schists possibly form a subduction complex, and the dunites are a good analogue to the mantle wedge overlying the slab. The Fujiwara dunites are of deserpentinization origin; the deserpentinized olivine is high in Fo (up to 96) and low in NiO (0.2 to 0.3 wt %), and contains magnetite inclusions. Titanoclinohumites are associated with the deserpentinized olivine, as lamellar intergrowth or veinlets, up to 1 cm in width. Other metamorphic minerals include antigorite, brucite, chlorite, ilmenite, perovskite, Ti-rich ludwigite, and carbonates. The protolith of the Fujiwara dunite was partially serpentinized cumulative dunites from intra-plate magma, containing relatively low-Fo (85 to 86) olivines and TiO_2-rich (up to 3 wt %) chromian spinels. The metamorphic olivines and titanoclinohumites contain micro-inclusions of methane (CH_4) with or without serpentine and brucite. The source of Ti for titanoclinohumite was possibly the Ti-rich chromian spinel, but Ti was mobile through hydrocarbon-rich fluids, which were activated during the metamorphism. The hydrocarbons, of which remnants are carbonates and methane micro-inclusions, were derived from carbonaceous materials or bitumen, possibly incorporated in the precursory serpentinized and brecciated peridotite (= the protolith for the Fujiwara dunites) before subduction. Ti can be mobile in the mantle wedge if hydrocarbons are available from the subducted slab.

1 Introduction

Titanium (Ti) is representative of high field strength elements (HFSE), and is believed to be immobile during aqueous fluid related processes (e.g., Tilley and Eggleton, 2005). In this context, most of HFSE in a subducting slab are transported along the base of mantle wedge to the deep mantle, which in part explains the HFSE depletion in

SED
4, 203–239, 2012

both arc mantle and magmas. However, Iizuka and Nakamura (1995) synthesized titanoclinohumite through interaction between metabasite and olivine at 850 °C and 8 GPa, with an orthopyroxene layer in between. Their experimental results indicated that Ti is mobile by aqueous fluid at least in a short range under high-P conditions. This implies a possibility of the presence of HFSE-enriched part within the mantle wedge.

Titanoclinohumite, one of mantle minerals (e.g., Aoki et al., 1976), contains both Ti and volatiles, and its genesis in peridotites is potentially important to consider the Ti mobility through metasomatism in the mantle. The simplified chemical formula of titanoclinohumite is $Ti_{0.5}Mg_{8.5}Si_4O_{17}$ (OH,F) and is thought as a kind mixture of olivine and brucite with minor amounts of TiO_2 (Jones et al., 1969). The TiO_2 content of titanoclinohumite is up to 6 wt % (Trommsdorff and Evans, 1980; Scambelluri et al., 1995; López Sánchez-Vizcaíno et al., 2005). Fluorine substitutes (OH) of titanoclinohumite and this substitution stabilizes titanoclinohumite at higher-temperature (800 °C or more) conditions (Engi and Lindsley, 1980). Titanoclinohumite has been occasionally reported from kimberlites (Aoki et al., 1976), peridotite xenoliths (Smith, 1979), and serpentinized peridotite bodies closely associated with high-P metamorphic rocks. Experiments of Engi and Lindsley (1980) indicated that the titanoclinohumites could be formed during metamorphism at crustal conditions: they are unstable above 475 °C at 0.35 GPa and 675 °C at 2.1 GPa.

Ishibashi et al. (1978) found titanoclinohumite in serpetinized dunites of Fujiwara ultramafic-gabbro complex in the Sanbagawa metamorphic belt, central Shikoku, Japan (Fig. 1). The ultramafic part of the Fujiwara complex is composed of dunite and wehrlite presumed as cumulates (e.g., Enami, 1980; Kunugiza, 1984). The Fujiwara dunite suffered deserpentinization during progressive Sanbagawa metamorphism and subsequent serpentinization during the exhumation. Ishibashi et al. (1978) described their petrographical features and interpreted the formation of titanoclinohumite was after recrystallization of olivine because of the replacive character (Ishibashi et al., 1978). The Fujiwara serpentinite-metagabbro complex has been studied by Onuki et al. (1978) and Enami (1980) to more constrain the Sanbagawa metamorphism.

SED
4, 203–239, 2012

However, no papers have thoroughly explained the petrogenesis of Fujiwara dunite and Ti source for the formation of titanoclinohumite.

In this paper, we describe the details of chemical features of Fujiwara titanoclinohumite, and discuss the Ti source and the formation process of titanoclinohumite in the dunite. It is quite important to understand what kind of fluid was involved in mobilization and concentration of HFSE. We can expect interaction between the Fujiwara complex and the Sanbagawa metamorphic rocks, especially an invasion of fluids released from Sanbagawa schists into the Fujiwara dunite during progressive metamorphism. This interaction possibly mimics slab/mantle wedge interaction; The titanoclinohumite formation in the Fujiwara dunite is, therefore, highly relevant to the mobility Ti within the mantle wedge.

2 Geological background

We examined titanoclinohumite-bearing dunites from the Fujiwara complex in the Sanbagawa metamorphic belt, central Shikoku, Japan (Fig. 1). The Sanbagawa belt is a regional metamorphic belt, of high-P intermediate metamorphic grade, extending approximately 800 km from east (Kanto district, north to Tokyo) to west (Saganoseki Peninsula, Kyushu) (Fig. 1a). The timing of peak metamorphism of the Sanbagawa belt was determined as 132–112 Ma (e.g., Okamoto et al., 2004). Abundant amphibolites, serpentinite and serpentinized ultramafic rocks and their complexes are distributed in the Sanbagawa metamorphic belt (e.g., Kunugiza 1984), and many studies have been published on P-T trajectories of the peridotites in the context of the subduction/exhumation history of the Sanbagawa metamorphic complex (e.g., Enami et al., 2004; Mizukami and Wallis, 2005). Maximum pressure recorded in garnet pyroxenites at Gongen area in the Sanbagawa metamorphic belt is 2.9–3.8 GPa at 700–810 °C (Enami et al., 2004). Based on petrological and geochemical features, some of the serpentinites were interpreted as fragments of the mantle wedge incorporated into the subduction complex (e.g., Hattori et al., 2010). On the other hand, some others were

SED
4, 203–239, 2012

originally in the oceanic lithosphere before incorporation into the subduction complex (e.g., Isozaki et al., 1990).

The Fujiwara metagabbro-ultramafic complex (less than 200 × 400 m in plan view) is situated within the Sanbagawa metamorphic belt on the central Shikoku Island, Japan (Fig. 1; Onuki et al., 1978). This is one of the representatives of a subducting slab complex, and will give us information about the mantle wedge above the slab (e.g., Scambelluri et al., 2001; Khedr and Arai, 2009). Host metamorphic rocks around the Fujiwara complex are mainly pelitic schists of the Ojoin Formation of the Sanbagawa belt, which belong to the high-P part of biotite zone to garnet biotite transition zone (Enami, 1980). The foliation of the Fujiwara complex is consistent with the schistosity of the surrounding pelitic schists (Enami, 1980; Onuki et al., 1987). The Fujiwara complex is composed of dunite, wehrlite and metagabbros, and wehrlitic lenses were observed within the gabbro (Fig. 1c; Onuki et al., 1978). The relationship between the dunite and gabbros is not clear, but the latter are possibly enclosed as a lens (<50 m in thickness) within the former (Onuki et al., 1978). Based on the detailed observations by Onuki et al. (1978), wehrlite is only found at the central part of the Fujiwara complex, and the relationship between the dunite and wehrlite is also unclear. Titanoclinohumite was only observed in the dunite part of the Fujiwara complex. The dunite is overall massive except for the western and eastern marginal parts of the body, where it is brecciated (Onuki et al., 1978). Unfortunately, the main part of the Fujiwara complex has been covered with a dam lake for hydroelectric generation (the Fujiwara dam), and cannot be directly observed anymore. Titanoclinohumites were first described from the Fujiwara complex by Ishibashi et al. (1978), who ascribed the production of titanoclinohumites and associated minerals to thermal metamorphism by some hidden thermal source (attributed to granitic intrusions).

SED
4, 203–239, 2012

3 Sample descriptions

We examined titanoclinohumite-bearing dunite samples from the northern end of marginal dunite of 7 samples of Fujiwara complex (cf. Onuki et al., 1976). The Fujiwara dunites examined in this study are highly serpentinized (cf. Fig. 2a–d) and mainly composed of olivine, chromian spinel and titanolinohumite with minor amount of chlorite, brucite, carbontates (dolomite and Ca carbonate), clinopyroxene, ilmenite and titanite, except for antigorite serpentine. The titanoclinohumite-bearing dunites show a peculiar breccia-like texture (cf., Ishibashi et al., 1978): a coarse-grained matrix includes strongly to completely serpentinized dunite clasts (Fig. 2a–b, e–f). Most of titanoclinohumite grains are exclusively observed in the coarse-grained matrix of olivine (Fig. 2a, b). The coarse-grained matrix exhibits strong deformation; both olivine and titanoclinohumite grains are kinked (cf. Fig. 2b). Olivines as well as titanoclinohumites are characterized by minute inclusions of magnetite as well as colorless fluids (Fig. 2g, h). The dunite clasts mainly comprise antigorite laths and brucite aggregates. Penetration of antigorite laths form ragged grain boundaries of relict olivine grains in the matrix part (Fig. 2g). The dunite is abundant in euhedral chromian spinels, both in the dunite clast and in the matrix, which are 4 %, on average, in volume (Fig. 2a, c, i–k). Spinels form composite grains; chromian spinel cores were thinly rimmed by ferritchromite and magnetite outward, each boundary being quite sharp (Fig. 2j, k). Both olivine and titanoclinohumite grains are in direct contact with the magnetite rim of the composite spinel grains in the matrix part (Fig. 2j–m). Chlorite is characteristically observed as coarse discrete grains (Fig. 2n), not always associated with altered chromian spinel as usually observed in metamorphosed peridotites (cf. Khedr and Arai, 2010). Magnetite is disseminated in whole part of the thin sections, and also in olivine as minute inclusions (Fig. 2a, g–h). Brucite is usually observed as veinlets crosscutting antigorite aggregates (Fig. 2i).

As stated above, titanoclinohumite grains are almost exclusively associated with olivine, as inclusions, veinlets replacing olivine and lamella-like thin intergrowths

SED
4, 203–239, 2012

(Fig. 2g, l, n–o). Some titanoclinohumite grains are also closely associated with magnetite and ilmenite (Fig. 2p, q). The grain boundary of titanoclinohumite is usually clear but rarely altered to titanite in contact with antigorite. We could not observe, however, any replacement textures by olivine and ilmenite, which were reported in other titanoclinohumite-bearing ultramafics (e.g., Trommsdorff and Evans, 1980). Titanoclinohumite was also observed as discrete grains and veinlets in the serpentinized dunite clasts (Fig. 2r). The veins are usually narrow (100–200 µm), but rarely exceed 1 cm in width (Fig. 2c–d). Wide vein contains abundant Ti-rich minerals, such as perovskite ($CaTiO_3$), ilmenite, and Ti-bearing borate (ludwigite; $(Mg,Fe)_2(Fe,Ti,Mg)BO_5$). The Ti-bearing ludwigite shows fibrous shapes and forms aggregates with magnetite surrounded by brucite.

4 Mineral chemical features

4.1 Major-element compositions

We determined major-element compositions, using the electron microprobe (EPMA) at Kanazawa University. For quantitative analysis of major elements, we used JXA-8800R (JEOL), and the accelerating voltage, beam current and probe diameter was 20 kV, 20 nA, and 3 µm, respectively. For map analysis, we used the same accelerating voltage with 50 nA beam current and 0 µm probe diameter. Counting time for each elements on quantitative analysis, we took 30 s and 15 s for peak and background for Ni, respectively, and 20 s and 10 s, respectively, for other elements (cf. Table 1). Ferrous and ferric iron contents of chromian spinel were calculated assuming spinel stoichiometry, while all iron was assumed to be Fe^{2+} in silicates. Mg# is Mg/(Mg + Fe^{2+}) atomic value, and Cr# is Cr/(Cr + Al) atomic value. Fluorine is an important component of titanoclinohume, but we did not measure the F content quantitatively, because there were no perceptible peaks for F in a preliminary qualitative analysis.

SED
4, 203–239, 2012

The olivines show a wide range of Fo content even within a single specimen, from 88 to 96 (Fig. 3). The MnO content of olivine is high, up to 1.1 wt %, and shows a negative correlation with the Fo content (Fig. 3a). The CaO content of olivine is generally low <0.2 wt %. The NiO content of olivine varies from 0.2 to 0.5 wt %, being characterized by remarkably low content (0.2 to 0.3 wt %) even at high Fo content (≈95) (Fig. 3b). The Cr# of spinel core (cf. Fig. 2j) is 0.5–0.6, and the TiO_2 content varies from 0.8 to 3.5 wt % (Fig. 4). The TiO_2 content of spinel is negatively correlated with Fe^{3+}/(Cr + Al + Fe^{3+}) atomic value, which varies from 0.3 to 0.2 (Fig. 4c). The TiO_2 content is lower than 1 wt % in ferritchromite and marginal magnetite (Fig. 4c). The MnO content is around 1 wt % in the spinel core, less than 1 wt % in the marginal magnetite, and relatively high, from 2 to 3 wt %, in ferritchromite (Table 1). It is noteworthy that the chromian spinel tends to be more severely altered to magnetite, i.e. becomes Ti-poorer, when it is associated with titanoclinohumite than in serpentine aggregates (Fig. 2k).

Titanoclinohumites show a wide variation of chemical composition (Table 1; Fig. 5). The oxide total in microprobe analysis ranges from around 99 to 95 wt %, being negatively correlated with the TiO_2 content, 2 to 8 wt % (Fig. 5a, b). The result of qualitative analysis indicates that the anion of titanoclinohumite in the Fujiwara dunite is mainly hydroxyl, which is consistent with the result of precursory work by Ishibashi et al. (1978). In addition, Jones et al. (1969) argued that the high-Ti character (TiO_2 > 1.9 wt %) of clinohumite is associated with low-F concentrations because of its crystallographic constraints. The Fujiwara titanoclinohumites are quite TiO_2-rich (up to 8 wt %) when they are in contact with ilmenite or perovskite (cf. Fig. 2q). Titanoclinohumites are basically magnesian, and their Mg# varies from 0.92 to 0.96, (Fig. 5a–d). Their NiO and MnO contents are overall low, <0.5 wt % (mostly around 0.2 wt %) and 0.2 to 0.6 wt %, respectively (Fig. 5c, d). For the Ti-rich varieties the Ti content is negatively correlated with the Si content, possibly indicating a substitution of Ti for Si (Fig. 5e). Ti is negatively correlated with (Fe + Mn + Mg + Ni) for the main cluster of titanoclinohumites, indicating substitution of Ti for M^{2+} (divalent cations) (Fig. 5f).

SED
4, 203–239, 2012

Irrespective of the mode of occurrences, chlorite shows almost constant Mg# and Al_2O_3 content, around 0.95 and 11.0–12.7 wt %, respectively (Table 1). Carbonates are dolomite and Mg-bearing Ca carbonate, of which MgO content is up to 4 wt %. Brucite has high Mg# (0.97–0.98) and contains a small amount of FeO and NiO, 2.5–3.7 wt % and 0.24–0.28 wt %, respectively (Table 1). The TiO_2 content and Mg# of Ti-bearing ludwigite varies from 2.7 to 3.8 wt % and 0.39 to 0.41, respectively (Table 1).

4.2 Trace-element compositions

We used a laser-ablation system inductively coupled plasma mass spectroscopy (LA-ICP-MS) at Kanazawa University to determine trace-element characteristics of minerals; the laser-ablation system and mass spectrometer was GeoLas Q-Plus (MicroLas) and Agilent 7500S (Yokogawa Analytical Systems), respectively. We used a laser energy density of 8 J/cm^2 operating at a frequency of 5 Hz. The laser spot size was 40 µm for ilmenite and petovskite, and 100 µm for olivine and titanoclinohumite. The NIST 612 standard glass was used for calibration with Si as an internal standard. Details of the analytical methods have been described by Ishida et al. (2004) and Morishita et al. (2005).

We checked incompatible trace-element concentrations of major Ti-rich phases (titanoclinohumite, ilmenite and perovskite) and olivine, to find which kind of elements were mobile with Ti. REE patterns of titanoclinohumites, normalized to primitive-mantle values of McDonough and Sun (1995), are quite similar to those of olivine except for positive spikes at HFSE of titanoclinohumites (Fig. 6a, b). Ilmenite is quite rich in Ti but shows almost the same concentrations as titanoclinohumites for other HFSE (Fig. 6b, c). Pervoskite shows, however, quite enriched patterns with strong negative spikes at Pb, some LILE (Rb, Ba and Sr) and HFSE (Zr and Hf) (Fig. 6c). HFSE variations in the Fujiwara titanoclinohumites are shown in Fig. 7. Their Ta and Nb contents are quite high relative to the Fujiwara olivines, although they are fairly low relative to titanoclinohumites from Almirez (López Sánchez-Vizcaíno et al., 2005). On the other hand, concentrations of Zr and Hf are fairly high relative to those in both of the Almirez

SED
4, 203–239, 2012

titanoclinohumites and the Fujiwara olivines (Fig. 7). The chondrite-normalized HFSE ratio (Ti, Nb and Zr) of titanoclinohumite shows their Ti/Nb variations with low Zr/Ti and Zr/Nb ratios (<0.1) (Fig. 7c). Titanoclinohumites from other localities, China (Zhang et al., 2007), Almirez (Garrido et al., 2005) and western Alps (Scambelluri et al., 2001), also show low Zr and variable Ti/Nb ratios. The titanoclinohumite from China shows a low Ti/Nb ratio due to the extremely high Nb concentration (84.8 ppm) (Zhang et al., 2007).

4.3 Raman spectroscopy

We performed Raman spectroscopy to identify fluid inclusion phases, using a micro-Raman system LabRAM HR800 (HoRIBA Jobin Yvon) equipped with a 532 nm Nd:YAG laser J100GS-16 (Showa Optronics CO., Ltd.). The laser beam was narrowed and focused through a 100 μm entrance pinhole and a 100× objective lens MPLN100x, NA = 0.90, (Olympus). We basically used a 600 lines/mm grating, but for specific analysis, we used 1800 lines/mm grating. Before measurements, the spectrometer was calibrated by using the Si 520 cm^{-1} peak. It was verified that the peak centers of neon lines are reproduced with precisions lower than 0.5 cm^{-1}. Details of the methods are in Miura et al. (2011).

We checked minute fluid inclusions (micro-inclusions) both in olivine and titanoclinohumite (Fig. 8). They are characteristically irregular, sometimes ameboid, in shape (Fig. 8), and distributed at random within grains, possibly indicating a primary character. The inclusions are colorless and homogeneous in appearance under the microscope (Fig. 8). Raman spectra from the micro-inclusions show a very strong peak at around 2907 cm^{-1}, varying from 2906 to 2910 cm^{-1} (Fig. 8), indicating fluid methane filling them. The methane is coexisting with serpentine and/or brucite irrespective of the host minerals. Some inclusions in titanoclinohumite are free of fluid phases and mainly comprise brucite with or without serpentine.

SED
4, 203–239, 2012

5 Discussion

5.1 Chemical characteristics of the Fujiwara titanoclinohumite

The Fujiwara titanoclinohumites display quite high TiO_2 contents (up to 8 wt %), showing a negative correlation with the oxide total by microprobe (Fig. 5a). This indicates that the Ti substitution in titanoclinohumite is not only with M (divalent cations), although Ti usually substitutes for their $Mg(OH)_2$ (brucite) component (Jones et al., 1969). To check the Ti substitution in the Fujiwara titanoclinohumites, we examined relations of the atomic ratio between Ti and M (divalent cations) and Ti and Si. Most of our analyses are plotted on the ideal substitution line of Ti-M with some exceptions (Fig. 5e–f). According to the ordinary stoichiometry of titanoclinohumite, the cation ratio of Ti should be below 0.49 on the basis of O = 17, although some Fujiwara titanoclinohumites exceed this value (up to 0.67) (Fig. 5f). This high-Ti character indicates the presence of $Mg(OH,F)_2$-TiO_2 layers replacing Mg_2SiO_4 layers (i.e., substitution of Ti(OH) with SiO_2), suggested by Bradshaw and Leake (1964), in the Fujiwara titanoclinohumites. If so, the titanoclinohumites will be non-stoichiometric when the $Mg(OH,F)_2$-TiO_2 layer exists, that is, when they are Ti-rich. This is consistent with the low oxide total for the TiO_2-rich titanoclinohumites (Fig. 5a, e–f). This possibly indicates the low availability of Si during the formation of titanoclinohumite.

5.2 Ti source for the formation of titanoclinohumite

As mentioned above, there have been several reports on titanoclinohumite-bearing ultramafics, of which the original lithology is mostly lherzolite or pyroxenites (e.g., Zhang et al., 1995; Garrido et al., 2005). Trommsdorff and Evans (1980) ascribed the Ti source for titanoclinohumite in the Malenco sepentinite to clinopyroxene in its protolith because of the strong association of the mineral with metamorphic clinopyroxene and chlorite. Clinopyroxene is important as a sink of Ti in mantle peridotites because of the strong preference of Ti to clinopyroxene (McDonough et al., 1992). Chromian spinel

SED
4, 203–239, 2012

is also an important container of TiO_2 in peridotites, especially when clinopyroxene is absent. It occasionally shows high TiO_2 contents, up to 12 wt % in cumulative dunites from oceanic hotspots (Arai et al., 2011). Chromian spinel was possibly a source of Ti for titanoclinohumite in the Fujiwara dunite, which had originally contained high-TiO_2 (up to 3.5 wt %) chromian spinel (Fig. 4c). Release of Ti from the primary chromian spinel during metamorphism is clear;s the spinel core decreases its TiO_2 content towards the magnetite rim (<0.5 wt %) through the ferritchromite (around 1.0 wt %) in between (Figs. 2k, 4). The rugged outline of the magnetite rim indicates later addition of magnetite around primary chromian spinel from surrounding olivine on serpentinization (e.g., Barnes, 2000). Ferritchromite was formed by modification of primary chromian spinel during serpentinization due to subtraction of the $MgAl_2O_4$ spinel component by forming chlorite and/or other hydrous minerals, although chromian spinel with chlorite is not so common. (Fig. 2e, i). The degree of conversion of chromian spinel to magnetite is high even though it is huge in size (≈500 µm) when closely associated with titanoclinohumite (Fig. 2l, m). In Contrast, chromian spinel is well preserved in the dunite clast, where titanoclinohumite has not been found (Fig. 2e, f).

We also examined ilmenite and/or perovskite coexisting with titanoclinohumite as a possible source of Ti. Elemental distribution maps of titanoclinohumite with ilmenite or perovskite show no systematic Ti enrichement towards them (Fig. 2q). The TiO_2 content is just averaged value (≈3 wt %) in some titanoclinohumite grains in contact with these Ti-rich phases. Assemblage of ilmenite and olivine can form titanoclinohumite at relatively high-P and low-T conditions (e.g., 600 °C and >14 kbar) (Engi and Lindsley, 1980). We did not find, however, any textures indicating reaction relation between them (Fig. 2q): the shape and size of ilmenite are euhedral and ≈120 µm, respectively. Perovskite also has euhedral shapes even in the wide titanoclinohumite vein. Chromian spinel is the most probable source of Ti to form titanoclinohumite and these Ti-rich phases in the Fujiwara dunites.

We examined the Ti budget for three thin sections. We measured modal amounts of titanoclinohumite, and opaque minerals by image processing. We assumed that

SED
4, 203–239, 2012

(1) all opaque grains (>100 µm) are spinel group minerals, (2) the volume of primary chromian spinel is equal to that of the present opaque grain (overgrown magnetite is negligible), (3) the degree of conversion of chromian spinel to magnetite is the same in every grain, and (4) the TiO_2 content of all chromian spinel and magnetite is 2.2 wt % and 0.45 wt %, respectively (averaged values) (cf. Fig. 4). The total modal amount of opaque minerals varies from 2 to 8 vol. %, and the averaged degree of conversion of chromian spinel to magnetite is almost constant (≈50 %). The sample containing 7 vol. % opaque minerals (T4-4) can supply an amount of TiO_2 sufficient to crystallize 0.6 vol. % titanoclinohumite. The other two samples (T4-1 and T4-3) contain too small amount of chromian spinel to provide titanoclinohumite with sufficient amounts of Ti. This indicates that, although chromian spinel is possibly the source of Ti, an external source for Ti is indispensible for formation of titanoclinohumite within a limited volume of the sample.

Comparing with titanoclinohumites from other localities (China, Almirez and western Alps), the Fujiwara titanoclinohumites is apparently low in Nb and Ta (Fig. 7a). On the other hand, Zr and Hf contents of the Fujiwara titanoclinohumites are higher than those from Almirez (Fig. 7b). These differences of the HFSE concentrations possibly reflect the difference of the source of HFSE to form titanoclinohumite. For example, residual clinopyroxenes of spinel lherzolite have high concentrations of Zr and Ti relative to secondary clinopyroxenes in Erro-Tobbio peridotites (Scambelluri et al., 2001). Additional data of HFSE concentrations in chromian spinel would be needed for further discussion.

5.3 Titanoclinohumite formation process and HFSE mobility

The primary Fujiwara dunites are characterized by the high-Ti chromian spinel and relatively low Fo content of olivine (Fo_{87}; Enami, 1980) or bulk-rock Mg# (0.85–0.87; Onuki et al., 1978). They were possibly cumulates from an intra-plate basalt (Arai et al., 2011) (cf. Figs. 3 and 4). The Fujiwara dunites are possibly of deserpentinization origin. The highly variable Fo content of olivine is one of characteristics of deserpentinized

SED
4, 203–239, 2012

peridotites (cf. Arai, 1975); Fujiwara dunites are a mixture of olivines of various origins. Inclusion of magnetite in olivines is also one of petrographical characteristics of deserpentinized peridotites (Arai, 1975). The lamellar intergrowth of titanoclinohumite in high-Mg# olivines indicates their simultaneous crystallization upon deserpentinization. Although the behavior of Ti during the precursory serpentinization process is not clear, the titanoclinohumite and other high-Ti phases (perovskite and ilmenite) were formed at the expense of the released Ti from primary Ti-rich spinels.

The presence of borate (high-Ti ludwigite) is also consistent with the serpentinization-deserpentinization imposed on the Fujiwara dunites. Serpentine minerals are one of the repositories of B in hydrous ultramafic rocks (Tenthorey and Hermann, 2004), and B is expected to be released during the breakdown process of serpentine. Antigorite, titanoclinohumite and chlorite actually contain quite high amounts of B (up to 11 000 ppm) (cf. Table 1), which are rather high compared with marine pelagic clays (230 ppm; Li, 1991). Boron has been available from outside of the Fujiwara dunite body, from, for example, the surrounding Sanbagawa pelitic schists. Breakdown of serpentinite and progressive metamorphism of the Sanbagawa metamorphic rocks produced high-B aqueous solutions, which affected the petrografic and chemical characteristics of the Fujiwara dunites. The solution was possibly rich in hydrocarbons; fluid inclusions in both titanoclinohumite and olivine are methane with brucite and/or serpentine (Fig. 8). The presence of brucite and/or serpentine in methane-rich fluid inclusions is interpreted as a reaction product between the host olivine or titanoclinohumite with the H_2O-CH_4 fluid as follows:

$$4Mg_2SiO_4 + 6H_2O = 2Mg_3Si_2O_5(OH)_4 + 2Mg(OH)_2 \text{ (in olivine)} \quad \text{(R1)}$$

$$3Mg_9Si_4O16(OH)_2 + 18H_2O = 6Mg_3Si_2O_5(OH)_4 + 9Mg(OH)_2 \text{ (in clinohumite)} \quad \text{(R2)}$$

Methane was involved in these reactions and remained as the main phase of the fluid inclusions. It has been well known that Ti is mobile through hydrocarbon-rich fluids even at low temperature conditions (e.g., Pointer et al., 1989; Rasmussen and Glover, 1994; Cornu et al., 1999; Parnell 2004). The hydrocarbon-rich fluids when

SED
4, 203–239, 2012

in contact with Ti-bearing phases scavenged Ti and other transitional metal elements to transport as hydrocarbon complexes to other places (Parnell, 2004). Carbonates (dolomite and Ca carbonate), frequently coexisting with Fujiwara titanoclinohumite, are possibly a reaction product of the hydrocarbon-rich fluid and serpentinite. Calcium to form Ca carbonate and perovskite was also derived from outside of the Fujiwara dunite, especially from associated gabbros (cf. Fig. 1).

The presence of methane as fluid inclusions in both metamorphic olivines and titanoclinohumites, combined with the vein-like occurrences of titanoclinohumite, suggests mobility of Ti via hydrocarbon-rich aqueous solutions. The texture of the titanolinohumite-bearing dunites possibly indicates a breccia as their protolith: dunite clasts with matrix rich in carbonaceous materials or bitumen (cf. Parnell, 2004). The brecciation may have occurred before subduction near a trench where an intra-plate volcano was deeply disrupted after transportation by an oceanic plate. The condition for formation of the Fujiwara titanolinohumite-bearing dunite should be bracketed by two reactions; brucite + antigorite = forsterite + H_2O (Evans, 1977) and titanoclinohumite = forsterite + ilmenite + H_2O (Engi and Lindsley, 1980) (Fig. 9). The protolith for the Fujiwara dunite, i.e. partially serpentinized (brecciated) dunite, was dragged to depth to be deserpentinzied mainly within the stability field of titanoclinohumite (Fig. 9). Based on the discussion of Enami (1980), the lower limit of Sanbagawa metamorphism recorded in the Fujiwara complex is 0.6–0.7 GPa and 450 °C, and the lack of talc and breakdown texture of titanoclinohumite in Fujiwara duntie implies a P-T trajectory which is almost the same as the Bessi unit (Fig. 9). Although the detailed P-T trajectory for the Fujiwara dunite body has not been known, it was derived from a depth far shallower than that of the Higashi-akaishi ultramafic complex (Fig. 9; Mizukami and Wallis, 2005).

6 Conclusions and implications

This study indicates formation of titanoclinohumites together with deserpentinized olivine in a progressively deserpentinized dunite, suggesting some mobility of Ti

SED
4, 203–239, 2012

through the fluid/solution activated during metamorphism at at <1 GPa and ≈500 °C. Ti is possibly mobile via hydrocarbon-rich solutions as shown in some metamorphosed bitumen-rich sediments (e.g., Parnell, 2004). This is consistent with the vein-like concentrations of titanoclinohumite cutting olivine-rich matrix. Therefore, Ti can be liberated from the slab to the overlying mantle wedge via released hydrocarbon-rich fluids. Ti fixed in minerals, such as chromian spinel, in the mantle wedge peridotite can be also mobilized by hydrocarbon-rich fluids released from the slab. The transported Ti can be concentrated as titanoclinohumite within the mantle peridotite at relatively low-T conditions (Engi and Lindsley, 1980). Therefore, HFSE, including Ti, are, however, immobile by aqueous fluids from the slab to the mantle wedge, and may not be incorporated in the arc magma source because titanoclinohumite is stable around the subducting slab. In addition, if titanoclinohumite is unstable, HFSE sink will be succeeded to ilmenite or other Ti-rich phases, stable at higher pressure. Then, HFSE are concentrated in the subducting slab and/or mantle peridotite (or serpentinite) just above the slab.

Acknowledgements. This work was partly supported by Grant-in-Aid for Young Scientist (B) (21740375). We greatly appreciate T. Morishita and A. Tamura, Kanazawa University, for LA-ICP-MS analysis. Raman spectroscopy was supported by T. Mizukami and M. Miura, Kanazawa University. R. Sawada supported us with preparing thin sections. Comments of S. Buiter, a topical editor, were helpful to improve the first submitted manuscript.

References

Aoki, K., Fujino, K., and Akaogi, M.: Titanochondridite and titanoclinohumite derived from the upper mantle in the Buell Park kimberlite, Arizona, USA, Contrib. Mineral. Petrol., 56, 243–253, 1976.

Arai, S.: Contact metamorphosed dunite-harzburgite complex in the Chugoku District, western Japan, Contrib. Mineral. Petrol., 52, 1–16, 1975.

Arai, S., Okamura, H., Kadoshima, K., Tanaka, C., Suzuki, K., and Ishimaru, S.: Chemical characteristics of chromian spinel in plutonic rocks: implications for deep magma processes and discrimination of tectonic setting, Island Arc., 20, 125–137, 2011.

Barnes, S. J.: Chromite in komatiites, II, Modification during greenschist to mid-amphibolite facies metamorphism, J. Petrol., 41, 387–409, 2000.
Bradshaw, R. and Leake, B. E.: A chondrodite-humite-spinel marble from Sørfinnset near Glomfjord, northern Norway, Mineral. Mag., 33, 1066–1080, 1964.
Cornu, S., Lucas, Y., Lebon, E., Ambrosi, J. P., Luizão, F., Rouiller, J., Bonnay, M., and Neal, C.: Evidence of titanium mobility in soil profiles, Manaus, central Amazonia, Geoderma, 91, 281–295, 1999.
Enami, M.: Petrology of the Fujiwara mass and the surrounding pelitic schists in the Sanbagawa metamorphic belt, central Shikoku, J. Geol. Soc. Japan., 86, 461–473, 1980.
Enami, M., Mizukami, T., and Yokoyama, K.: Metamorphic evolution of garnet-bearing ultramafic rocks from the Gongen area, Sanbagawa belt, Japan, J. Metamor. Geol., 22, 1–15, 2004.
Engi, M. and Lindsley, D. H.: Stability of titanian clinohumite: experiments and thermodynamic analysis, Contrib. Mineral. Petrol., 72, 414–424. 1980.
Evans, B. W.: Metamorphism of alpine peridotite and serpentinite, Annu. Rev. Earth Planet. Sci., 5, 397–447, 1977.
Garrido, C. J., López Sánchez-Vizcaíno, V., Gómez-Pugnaire, M. T., Trommsdorff, V., Alard, O., Bodinier, J.-L., and Godard, M.: Enrichment of HFSE in chlorite-harzburgite produced by high-pressure dehydration of antigorite-serpentinite: implications for subduction magmatism, Geochem. Geophys. Geosys., 6, Q01J15, doi:10.1029/2004GC000791, 2005.
Hattori, K., Wallis, S., Enami, M., and Mizukami, T.: Subduction of mantle wedge peridotites: Evidence form the Higashi-akaishi ultramafic body in the Sanbagawa metamorphic belt, Island Arc., 19, 192–207, 2010.
Iizuka, Y. and Nakamura, E.: Experimental study of the slab-mantle interaction and implications for the formation of titanoclinohumite at deep subduction zone, Proc. Japan Academy, 71, 159–164, 1995.
Ishibashi, K., Miyahisa, M., and Sasaki, M.: Titanoclinohumite from Fujiwara complex in the Higashi-akaishi Mountainland, Shikoku, Japan. J. Min. Petrol. Econ. Geol., 73, 18–25, 1978 (in Japanese with English abstract).
Ishida, Y., Morishita, T., Arai, S., and Shirasaka, M.: Simultaneous in-situ multi-element analysis of minerals on thin section using LA-ICP-MS, The Sci. Rep. Kanazawa Univ., 48, 31–42, 2004.
Isozaki, Y., Maruyama, S., and Furuoka, F.: Accreted oceanic materials in Japan, Tectono-

SED
4, 203–239, 2012

physics, 181, 179–205, 1990.
Jones, N. W., Ribbe, P. H., and Gibbs, G. V.: Crystal chemistry of the humite minerals, Am. Mineral., 54, 391–411, 1969.
Khedr, M. Z. and Arai, S.: Hydrous peridotites with Ti-rich chromian spinel as a low-temperature forearc mantle facies: evidence from the Happo-O'ne metaperidotites (Japan), Contrib. Mineral. Petrol., 159, 137–157, 2010.
Kunugiza, K.: Metamorphism and origin of ultramafic bodies of the Sanbagawa metamorphic belt in central Shikoku, J. Min. Petrol. Econ. Geol., 79, 20–32, 1984 (in Japanese with English abstract).
Li, Y.-H.: Distribution patterns of the elements of the elemenets in the ocean: A synthesis, Geochim. Cosmochim. Acta, 55, 3223–3250, 1991.
López Sánchez-Vizcaíno, V., Trommsdorff, V., Gómez-Pugnaire, M. T., Garrido, C. J., Müntener, O., and Connolly, J. A. D.: Petrology of titanian clinohumite and olivine at the high-pressure breakdown of antigorite serpentinite to chlorite harzburgite (Almirez Massif, S. Spain), Contrib. Mineral. Petrol., 149, 627–646, 2005.
McDonough, W. F. and Sun, S.-S.: The composition of the Earth, Chem. Geol., 120, 223–253, 1995.
McDonough, W. F., Stosch, H.-G., and Ware, N. G.: Distribution of titanium and the rare earth elements between peridotitic minerals, Contrib. Mineral. Petrol., 110, 321–328, 1992.
Miura, M., Arai, S., and Mizukami, T.: Raman spectroscopy of hydrous inclusions in olivine and orthopyroxene in ophiolitic harzburgite: implications for elementary processes in serpentinization, J. Mineral. Petrol. Sci., 106, 91–96, 2011.
Mizukami, T. and Wallis, S. R.: Structural and petrological constraints on the tectonic evolution of the garnet-lherzolite facies Higashi-akaishi peridotite body, Sanbagawa belt, SW Japan, Tectonics, 24, TC6012, doi:10.1029/2004TC001733, 2005.
Morishita, T., Ishida, Y., Arai, S., and Shirasaka, M.: Determinaion of meltiple trace element compositions in thin (<30μm) lasers of NIST SRM 614 and 616 using laser ablation-inductively coupled plasma-mass spectrometry (LA-ICP-MS), Geostand. Geoanal. Res., 29, 107–122, 2005.
Okamoto, K., Shinjoe, H., Katayama, I., Terada, K., Sano, Y., and Johnson, S.: SHRIMP U-Pb zircon dating of quartz-bearing eclogite from the Sanbagawa belt, south-west Japan: implications for metamorphic evolution of subducted protolith, Terra Nova, 16, 81–89, 2004.
Onuki, H., Yoshida, T., and Suzuki, T.: The Fujiwara mafic-ultramafic complex in the Sanbagawa

SED
4, 203–239, 2012

metamorphic belt of Central Shikoku. 1. Petrolchemistry and rock-forming mineralogy, J. Min. Petrol. Econ. Geol., 73, 311–322, 1978 (in Japanese with English abstract).
Parnell, J.: Titanium mobilization by hydrocarbon fluids related to sill intrusion in a sedimentary sequence, Scotland, Ore Geol. Rev., 24, 155–167, 2004.
Pointer, C. M., Ashworth, J. R., and Simpson, P. R.: Genesis of coffinite and the U-Ti association in Lower Old Red Sandstone sediments, Ousdale, Caithness, Scotland, Mineral. Deposita, 24, 117–123, 1989.
Rasmussen, B. and Glover, J. E.: Diagenesis of low-mobility elements (Ti, REEs, Th) and solid bitumen envelopes in Permina Kennedy Group sandstone, Western Australia, J. Sediment. Res., A64, 572–583, 1994.
Sato, H.: Nickel content of basaltic magmas: identification of primary magmas and measure of the degree of olivine fractionation, Lithos, 10, 113–120, 1977.
Sato, H. and Banno, S.: NiO-Fo relation of magnesian olivine phenocryst in high-magnesian andesite and associated basalt-andesite-sanukite from northeast Shikoku, Japan. Bull. Volcanol. Soc. Japan, 2nd Ser., 28, 141–156, 1983.
Scambelluri, M., Müntener, O., Hermann, J., Piccardo, G. B., and Trommsdorff, V.: Subduction of water into the mantle: history of an Alpine peridotite, Geology, 23, 459–462, 1995.
Scambelluri, M., Rampone, E., and Piccardo, G. B.: Fluid and element cycling in subducted serpentinite: a trace-element study of the Erro-Tobbio high-pressure ultramafites, J. Petrol., 42, 55–67, 2001.
Smith, D: Hydrous minerals and carbonates in peridotite inclusions from the Green Knobs and Buell park kimberlitic diatreames on the Colorado Plateau, in: The mantle sample: inclusions in kimberlites and other volcanics, edited by: Boyd, F. R. and Meyer, H. O. A., American Geophys. Union, 345–356, 1979.
Takahashi, E.: Origin of basaltic magmas-implications from peridotite melting experiments and an olivine fractionation model-. Bull. Volcanol. Soc. Japan, 30, S17–S40, 1986 (in Japanese with English abstract).
Tenthorey, E. and Hermann, J.: Composition of fluids during serpentinite breakdown in subduction zones: evidence for limited boron mobility, Geology, 32, 865–868, 2004.
Tilley, D. B. and Eggleton, R. A.: Titanite low-temperature alteration and Ti mobility, Calys and Clay Minerals, 53, 100–107, 2005.
Trommsdorff V. and Evans, B. W.: Titanian hydroxyl-clinohumite: formation and breakdown in antigorite rocks (Malenco, Italy), Contrib. Mineral. Petrol., 72, 229–242, 1980.

SED
4, 203–239, 2012

Ulmer, P. and Trommsdorff, V.: Serpentine stability to mantle depths and subduction-related magmatism, Science, 268, 858–861, 1995.
Zhang, R. Y., Liou, J. G., and Cong, B. L.: Talc-, magnesite- and Ti-clinohumite-bearing ultrahigh-pressure mafic and ultramafic complex in the Dabie Mountains, China. J. Petrol., 36, 1011–1037, 1995.
Zhang, R. Y., Li, T., Rumble, D., Yui, T.-F., Li, L., Yang, J. S., Pan, Y. and Liou, J. G.: Multiple metasomatism in Sulu ultrahigh-P garnet peridotite constrained by petrological and geochemical investigations, J. Metamorphic Geol., 25, 149–164, 2007.

SED
4, 203–239, 2012

Table 1. Representative major-element compositions of minerals in Fujiwara dunites. FeO and Fe_2O_3 contents of spinels are calculated values (see text). core sp1 and core sp2 in T4-1 are the core and rim of a spinel grain, respectively (cf. Fig. 2k).

Sample No.	SP01										
	Ti-vein									du clast	
point No.	1-CH1	3-CH1-1	5-CH1	2-ant1	2-chl2	1-ldw1-2	5-pvs1	6-mt1	6-mt2	7-sp1-1 core_sp	7-sp1-2 mtl_F-cr
SiO2	36.92	37.43	33.54	33.72	35.24	0.90	0.10	0.03			0.15
TiO2	2.97	2.67	8.11	0.60	0.42	3.11	57.61	0.24	0.08	0.78	0.73
Al2O3		0.11	0.01	11.55	9.53	0.10	0.01	0.01	0.02	27.92	0.53
Cr2O3			0.02	0.87	0.26	0.57			0.48	30.98	25.68
Fe2O3								68.25	68.46	8.77	40.15
FeO	6.22	5.27	6.75	3.40	2.77	58.16	0.44	29.68	29.67	21.76	27.12
MnO	0.22	0.22	0.26	0.26	0.17	0.36	0.01	0.13	0.17	0.52	2.69
MgO	51.63	52.97	47.02	34.12	35.94	21.78	0.06	0.58	0.77	9.73	2.05
CaO	0.15	0.22	0.06	0.10	0.23	0.21	41.55	0.02	0.01		0.00
Na2O				0.13		0.20				0.01	0.07
K2O	0.90		0.00	0.14							
NiO	0.18	0.17	0.10	0.12	0.19	0.35	0.01	0.17	0.46	0.20	0.43
Total	99.46	100.85	95.88	87.33	87.99	101.19	99.79	99.11	100.12	100.67	99.60
B (ppm)	419	2.795		3.612	5.031	23.997					
Mg#	0.993	0.994	0.991	0.994	0.995	0.862	0.703	0.033	0.044	0.444	0.119
Cr#								0.000	0.947	0.427	0.970
Cr/R^{3+}								0.000	0.007	0.383	0.397
Al/R^{3+}								0.000	0.000	0.514	0.012
Fe^{3+}/R^{3+}								1.000	0.992	0.103	0.591

Abbreviations are as follows; CH, titanoclinohumite: ant, antigorite: chl, chlorite: ldw, ludwigite: pvs, perovskite: mt, magnetite: sp, spinel: F-cr, ferritchromite: ol, olivine: br, brucite: ilm, ilmenite: carb, carbonate.

SED
4, 203–239, 2012

Table 1. Continued.

Sample No.	T4-1										
point No.	1-ol1	1-ol2	3-CH1	2-br1	4-chl1	4-ant1	3-ilm1 in CH	1-sp1-1 core_sp1	1-sp1-2 core_sp2	1-sp1-3 mtl_F-cr	1-sp1-4 rim_mt
SiO2	40.69	40.53	34.35	0.11	35.23	43.43	0.02			0.03	0.01
TiO2	0.03	0.00	6.70	0.02			56.67	2.01	2.04	0.82	0.15
Al2O3					12.68	1.38	0.01	19.31	19.53	1.13	0.02
Cr2O3					0.03	0.65		34.12	34.04	30.02	0.92
Fe2O3								11.96	12.13	34.67	67.71
FeO	6.44	11.41	10.59	2.45	3.01	2.05	26.89	20.66	21.07	25.63	29.28
MnO	0.40	1.07	1.11	0.17	0.04	0.03	6.46	1.09	1.14	2.70	0.21
MgO	50.98	47.94	45.47	67.61	34.90	39.59	10.55	9.10	9.00	2.92	0.91
CaO	0.02	0.03		0.01	0.01					0.01	0.01
Na2O					0.00			0.00	0.00	0.05	0.05
K2O		0.00							0.00		
NiO	0.42	0.40	0.18	0.24	0.13	0.11	0.13	0.25	0.24	0.55	0.72
Total	98.96	101.39	98.40	70.62	86.03	87.25	100.72	98.50	99.20	98.53	99.98
Mg#	0.934	0.882	0.884	0.980	0.954	0.972	0.411	0.440	0.432	0.169	0.053
Cr#								0.542	0.539	0.947	0.967
Cr/R^{3+}								0.459	0.456	0.464	0.014
Al/R^{3+}								0.387	0.390	0.026	0.000
Fe^{3+}/R^{3+}								0.153	0.155	0.510	0.986

SED
4, 203–239, 2012

Table 1. Continued.

Sample No.	T4-3								
point No.	1-ol1	3-ol1	4-ol1	2-CH1	5-CH1	7-CH1	6-ant1	8-sp1-1 core_sp	8-sp1-2 rim_mt
SiO2	41.40	41.21	40.88	37.61	36.95	36.24	44.14	0.00	0.26
TiO2	0.03	0.04	0.01	4.42	3.55	5.44	0.03	2.81	0.07
Al2O3		0.00	0.00		0.01	0.00	0.59	19.59	0.01
Cr2O3		0.02	0.00		0.00	0.00	0.04	32.89	0.22
Fe2O3								13.28	68.66
FeO	7.42	7.28	9.49	6.05	9.29	8.87	1.51	21.88	29.01
MnO	0.39	0.36	0.62	0.25	0.63	1.00	0.03	0.91	0.18
MgO	51.81	51.51	49.67	50.80	48.31	47.12	39.75	8.88	1.12
CaO	0.00	0.02	0.01		0.02	0.01	0.01	0.00	0.00
Na2O	0.01	0.00	0.00	0.02	0.01	0.02	0.00	0.02	0.03
K2O	0.00	0.00	0.01		0.00	0.00	0.00	0.00	0.00
NiO	0.55	0.34	0.46	0.23	0.30	0.17	0.12	0.29	0.67
Total	101.61	100.77	101.16	99.38	99.07	98.87	86.21	100.54	100.23
Mg#	0.926	0.927	0.903	0.937	0.903	0.904	0.979	0.420	0.064
Cr#								0.530	0.931
Cr/R^{3+}								0.440	0.003
Al/R^{3+}								0.391	0.000
Fe^{3+}/R^{3+}								0.169	0.996

SED
4, 203–239, 2012

Table 1. Continued.

Sample No.	T4-4											
point No.	1-ol1	5-ol1	7-ol1	2-CH1	4-CH1	3-chl1	6-chl1-1	2-carb1	3-carb1	5-sp1-1 core_sp	5-sp1-2 mtl_F-cr	5-sp1-3 rim_mt
SiO2	42.22	41.01	41.99	37.27	37.25	35.07	34.72	0.76	0.04	0.00	0.00	0.04
TiO2	0.00	0.10	0.01	4.68	2.80	0.00	0.00	0.04	0.02	1.06	0.74	0.06
Al2O3	0.00	0.00	0.00	0.00	0.00	11.48	11.55	0.00	0.00	16.92	2.64	0.01
Cr2O3	0.02	0.00	0.00	0.00	0.00	0.52	0.40	0.13	0.05	34.91	31.75	0.02
Fe2O3										17.03	32.35	69.25
FeO	5.58	9.06	4.35	5.75	4.36	3.15	3.18	0.23	0.08	21.73	25.31	29.47
MnO	0.33	0.61	0.13	0.26	0.43	0.01	0.02	0.24	0.00	0.81	2.77	0.19
MgO	54.06	50.29	54.70	51.15	53.83	35.24	35.31	4.15	25.45	8.46	3.58	0.95
CaO	0.01	0.02	0.02	0.00	0.01	0.02	0.01	54.28	32.97	0.00	0.01	0.00
Na2O	0.00	0.02	0.00	0.01	0.00	0.00	0.00	0.02	0.03	0.00	0.02	0.00
K2O	0.00	0.00	0.01	0.00	0.00	0.00	0.01	0.00	0.01	0.00	0.00	0.00
NiO	0.38	0.44	0.29	0.20	0.16	0.11	0.10	0.03	0.00	0.28	0.46	0.76
Total	102.61	101.54	101.50	99.32	98.85	85.60	85.30	59.87	58.64	101.20	99.62	100.75
Mg#	0.945	0.908	0.957	0.941	0.956	0.952	0.952	0.969	0.998	0.410	0.201	0.054
Cr#										0.581	0.890	0.626
Cr/R^{3+}										0.457	0.478	0.000
Al/R^{3+}										0.330	0.059	0.000
Fe^{3+}/R^{3+}										0.212	0.463	1.000

SED
4, 203–239, 2012

Table 1. Continued.

Sample No.	T4-8										
point No.	1-ol1	3-ol1	6-ol1	2-CH1	5-CH2	4-carb4	7-carb1	6-ant1	7-chl1	7-sp1-1 core_sp	7-sp1-2 rim_mt
SiO2	40.47	41.44	41.61	37.02	41.53			44.09	35.24		
TiO2	0.03	0.02		3.31	0.22	0.01		0.03	0.01	3.41	0.14
Al2O3					0.00	0.01	0.00	0.40	10.95	19.70	
Cr2O3				0.02					0.42	34.97	1.23
Fe2O3										10.87	68.62
FeO	10.95	8.25	4.57	6.63	4.05	0.39	0.09	1.16	3.28	21.39	29.49
MnO	0.79	0.43	0.35	0.35	0.19	0.20	0.03	0.04	0.02	0.96	0.21
MgO	48.36	51.26	54.66	50.78	54.29	21.34	0.04	40.35	35.15	9.63	1.10
CaO	0.01	0.01	0.01	0.01	0.00	31.15	61.09	0.00	0.01	0.01	0.09
Na2O				0.01						0.01	0.03
K2O		0.01	0.00	0.00	0.01			0.01	0.00		
NiO	0.42	0.37	0.25	0.13	0.19	0.00	0.02	0.11	0.13	0.21	0.50
Total	101.04	101.78	101.44	98.25	100.49	53.09	61.27	86.18	85.20	101.16	101.40
Mg#	0.887	0.917	0.955	0.932	0.960			0.984	0.950	0.445	0.062
Cr#										0.544	1.000
Cr/R^{3+}										0.468	0.018
Al/R^{3+}										0.393	0.000
Fe^{3+}/R^{3+}										0.138	0.982

SED
4, 203–239, 2012

Table 1. Continued.

Sample No.	T4-19									
point No.	1-ol1	3-ol1	5-ol1	4-CH1	7-CH1	6-br1	2-carb1	3-mt1 in ol1	4-sp1-1 core_sp	4-sp1-2 rim_mt
SiO2	41.91	41.66	42.30	37.50	36.80	0.02	0.00	0.06	0.00	0.02
TiO2		0.00	0.00	3.66	4.47	0.01	0.03	0.19	1.10	0.13
Al2O3		0.01	0.00	0.00	0.00	0.00	0.01	0.00	18.75	0.00
Cr2O3		0.04	0.00	0.02	0.00	0.00	0.04	3.91	31.99	1.36
Fe2O3								63.52	17.68	67.88
FeO	5.67	7.85	5.22	4.97	7.03	3.67	0.18	28.17	22.02	29.45
MnO	0.23	0.55	0.23	0.32	0.62	0.23	0.21	0.36	0.94	0.20
MgO	52.01	52.62	54.57	51.74	49.71	66.81	1.71	1.26	8.42	0.97
CaO	0.01	0.03	0.02	0.01	0.01	0.01	60.00	0.00	0.00	0.00
Na2O		0.00	0.00	0.00	0.02	0.00	0.02	0.00	0.01	0.02
K2O		0.00	0.00	0.00	0.00	0.00	0.00	0.00	0.00	0.00
NiO	0.32	0.37	0.29	0.24	0.26	0.28	0.01	0.83	0.30	0.74
Total	100.15	103.12	102.62	98.46	98.91	71.03	62.21	98.30	101.21	100.77
Mg#	0.942	0.923	0.949	0.949	0.927	0.970	0.944	0.074	0.405	0.056
Cr#								1.000	0.534	1.000
Cr/R^{3+}								0.061	0.417	0.021
Al/R^{3+}								0.000	0.364	0.000
Fe^{3+}/R^{3+}								0.939	0.219	0.979

SED
4, 203–239, 2012

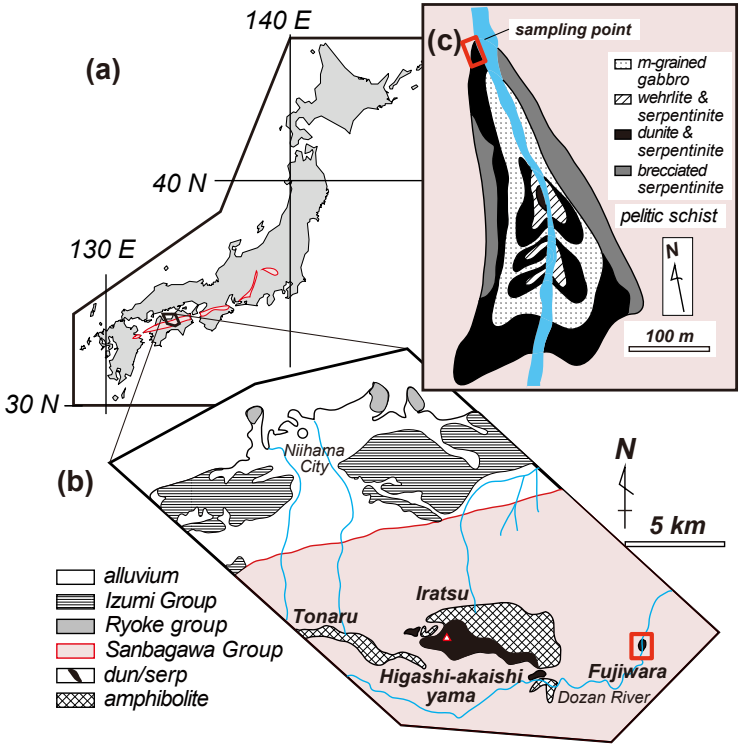

Fig. 1. Map showing the E-W extent of the Sanbagawa belt **(a)** and geology around the Fujiwara complex **(b, c)** modified after Ishibashi et al. (1978).

SED
4, 203–239, 2012

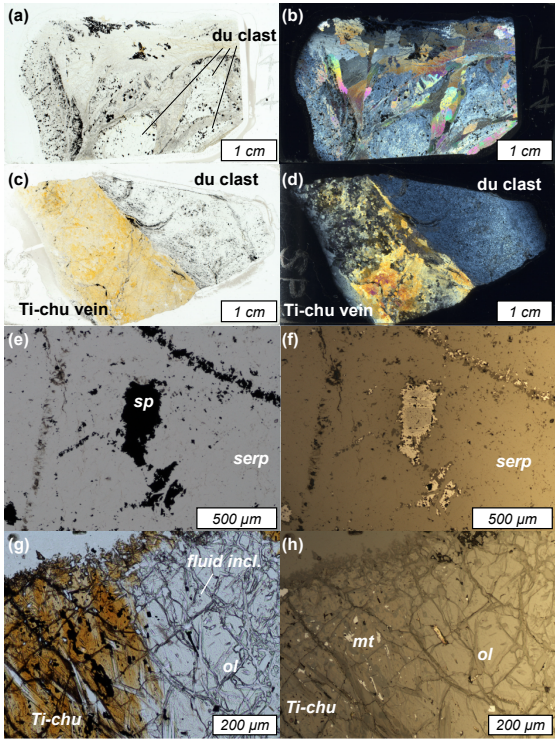

Fig. 2a. Photomicrographs (a–j, l–p, r) and Ti distribution maps (k, q) taken by microprobe of chromian spinel in Fujiwara dunite. Abbreviations are as follows: du, dunite: Ti-chu, titanoclinohumite: sp, chromian spinel: serp, serpentine: ol, olivine: fluid incl., fluid inclusion: mt, magnetite: br, brucite: F-cr, ferritchromite: chl, chlorite: and ilm: ilmenite. **(a)** Plane-polarized image of sample T4-4. Note that the brecciated texture. **(b)** Crossed-polarized image of **(b)**. Note the highly serpentinized dunite clasts and coarse olivines. **(c)** Plane-polarized image of sample SP1 containing thick titanoclinohumite vein. **(d)** Crossed-polarized image of **(c)**. **(e)** Subhedral spinel grain in serpentinized clast. Plane-polarized light image. **(f)** Reflected-light image of **(e)**. Note the bright magnetite rim around dark core of chromian spinel. **(g)** Intergrowth of olivine and titanoclinohumite with antigorite lath, magnetite and fluid inclusions. Plane-polarized light image. **(h)** Reflected light image of **(g)**. Minute magnetite grains are observed both in olivine and in titanoclinohumite. **(i)** Brucite vein cross-cutting dunite clast. Note the euhedral chromian spinel in the matrix olivine aggregate. Plane-polarized light image. **(j)** Reflected light image of chromian spinel in rectangular area of **(i)** . Bright magnetite rim and ferritchromite are observed around the chromian spinel. **(k)** Ti distribution map of chromian spinel in **(k)**. The Ti concentration decreases from the chromian spinel core to the magnetite rim the through ferritchromite mantle. **(l)** Opaque mineral (mt) in contact with relatively large titanoclinohumite. Plane-polarized light image. **(m)** Reflected-light image of **(l)**. Note that the opaque mineral is completely changed to magnetite. **(n)** Chlorite is observed in equilibrium with olivine, titanoclinohumite, magnetite and serpentine. Plane-polarized light image. **(o)** Lamellar titanoclinohumite in olivine. Plane-polarized light image. **(p)** Titanoclinohumite with euhedral ilmenite. Plane-polarized light image. **(q)** Ti distribution map of rectangle area **(p)**. **(r)** Titanoclinohumite vein in dunite clast. Opaque mineral in upper right is completely changed to magnetite from chromian spinel, although the primary chromian spinel has still preserved in the opaque mineral in lower left. Plane-polarized light image.

SED
4, 203–239, 2012

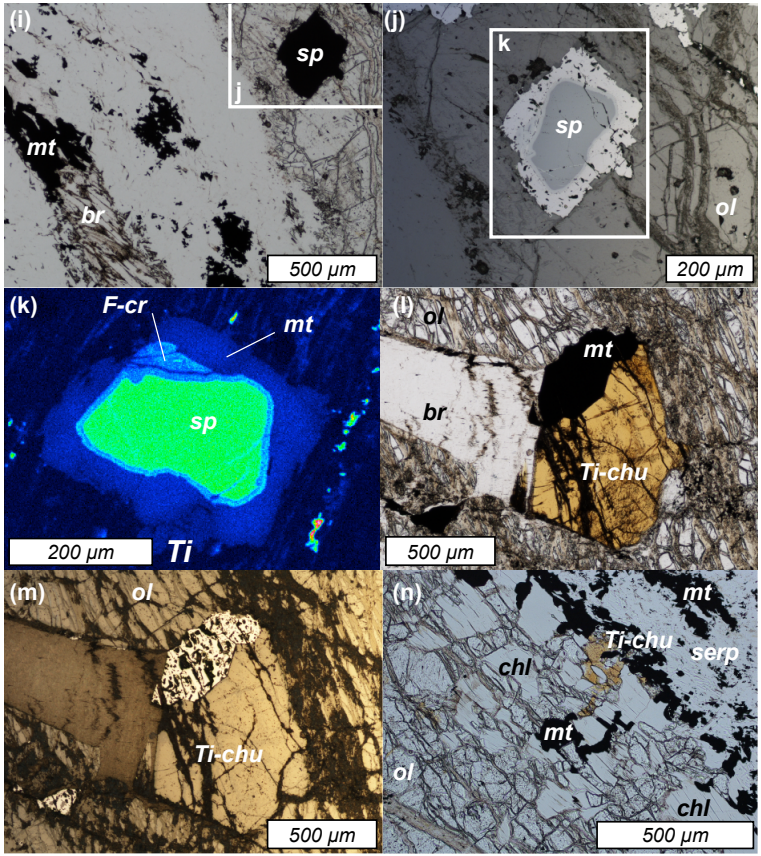

Fig. 2b. Continued.

SED
4, 203–239, 2012

Possibility of titanium transportation within a mantle wedge

S. Ishimaru and S. Arai

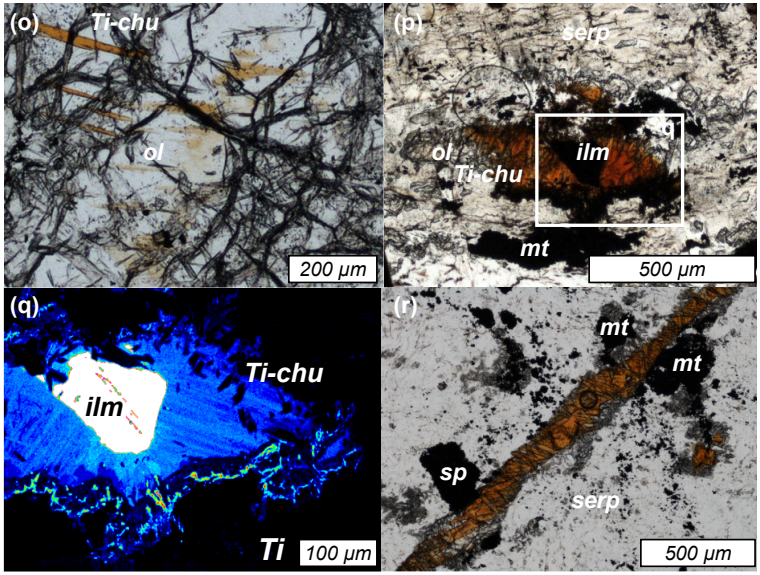

Fig. 2c. Continued.

SED
4, 203–239, 2012

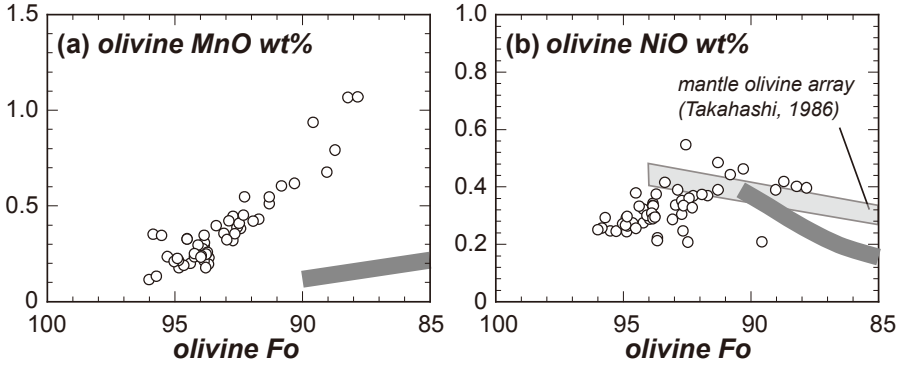

Fig. 3. Major-element variations of olivines in Fujwara dunites. **(a)** Relationships between the Fo content and MnO content. Thick gray line shows the fractional crystallization trend of Sato and Banno (1983). **(b)** Relationships between the Fo content and NiO content. Thick gray line and light gray area show the fractional crystallization trend and mantle olivine array of Sato and Banno (1983) and Takahashi (1986), respectively.

SED
4, 203–239, 2012

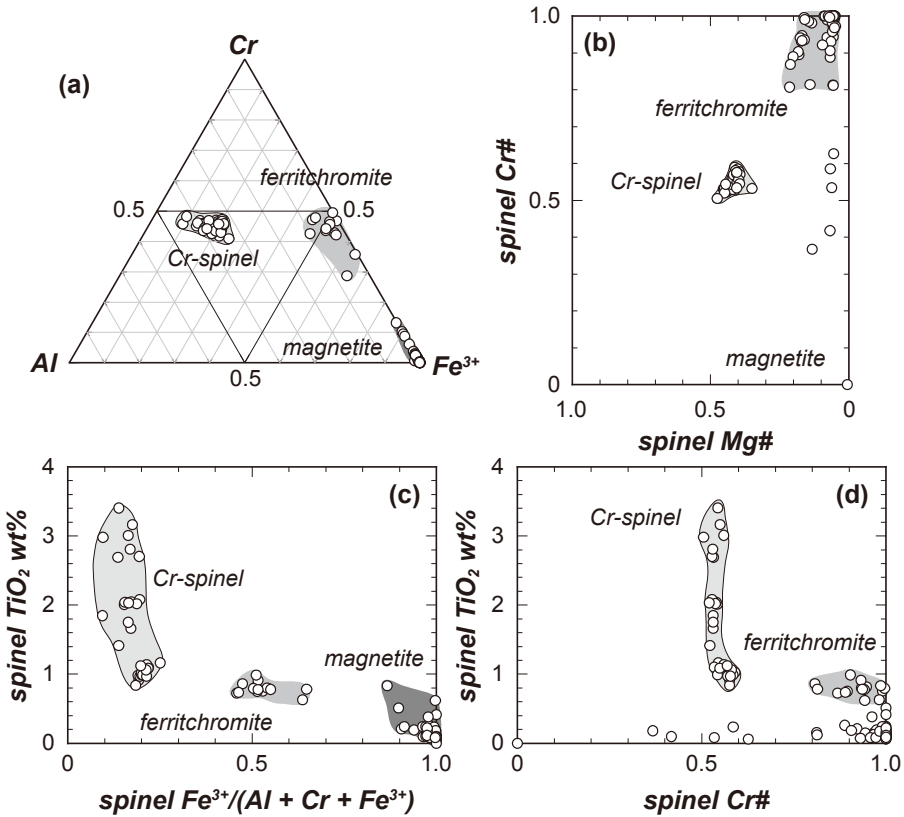

Fig. 4. Major-element variations of spinels (chromian spinel, ferritchromite and magnetite) in Fujwara dunites. **(a)** Trivalent cation ratios. **(b)** Relationships between Mg# and Cr#. **(c)** Relationships between the Fe^{3+} ratio and TiO_2 content. **(d)** Relationships between Cr# and TiO_2 content.

SED
4, 203–239, 2012

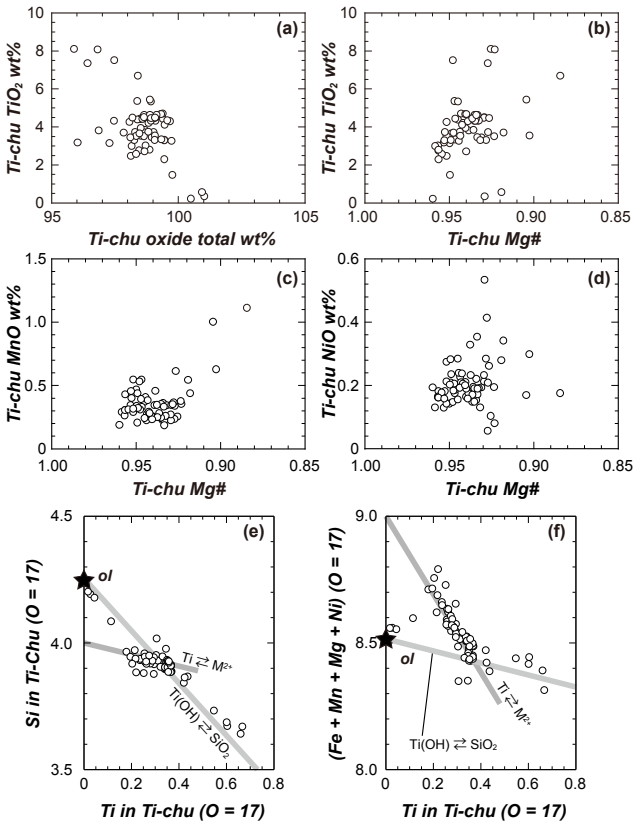

Fig. 5. Major-element variations of titanoclinohumites in Fujwara dunites. **(a)** Relationships between the oxide total in microprobe analysis and TiO_2 content. **(b)** Relationships between Mg# and TiO_2 content. **(c)** Relationships between Mg# and MnO content. **(d)** Relationships between Mg# and NiO content. **(e)** Relationships between the cation ratios of Ti and Si. **(f)** Relationships between the cation ratio of Ti and divalent cations (Fe, Mn, Mg and Ni).

SED
4, 203–239, 2012

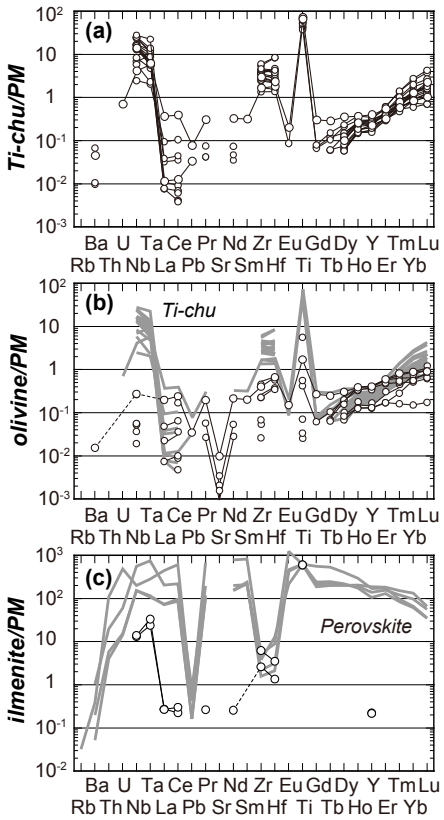

Fig. 6. Trace-element patterns of minerals, normalized to primitive-mantle values (McDonough and Sun, 1995). **(a)** Titanoclinohumites. **(b)** Olivines. Patterns of titanoclinohumite are also shown (gray) for comparison. **(c)** Ilmenite and perovskite (gray).

SED
4, 203–239, 2012

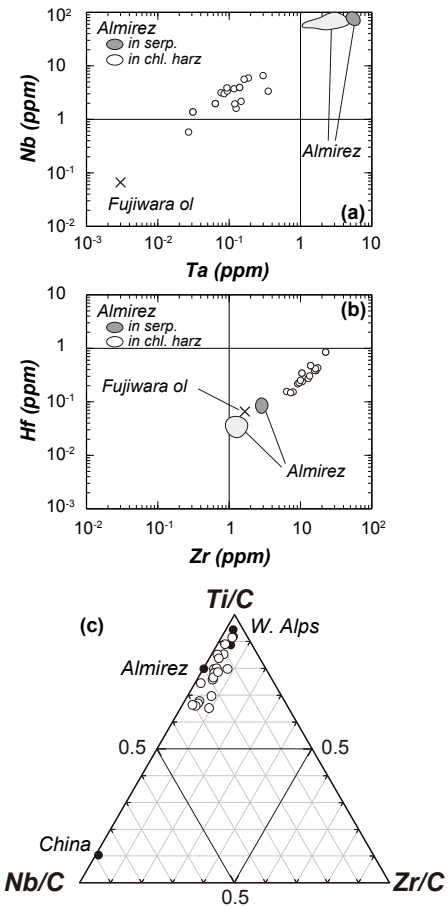

Fig. 7. HFSE variations in titanoclinohumites from Fujiwara dunites. Data of titanoclinohumites from other localities are also shown for comparison: Almirez (López Sánchez-Vizcaíno et al., 2005), Westetrn Alps (Scambelluri et al., 2001) and China (Zhang et al., 2007). Chondrite values for normalization are from McDonough and Sun (1995).

SED
4, 203–239, 2012

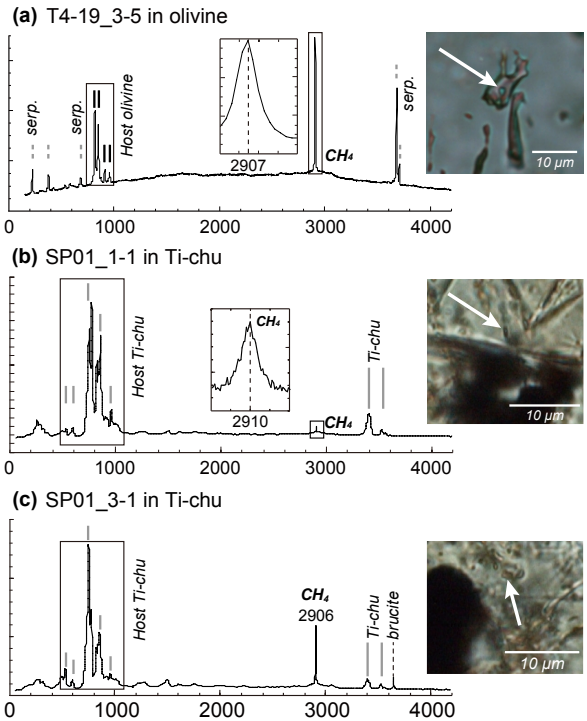

Fig. 8. Results of Raman spectroscopy. Horizontal and vertical axes show wave numbers (cm^{-1}) and intensity, respectively. **(a)** Inclusion in olivine in sample T4–19. The fluid inclusion showing an irregular shape indicates the coexistence of serpentine and methane in olivine. **(b)** Inclusion in titanoclinohumite in sample SP01. **(c)** Inclusion in titanoclinohumite in sample SP01. Brucite coexists with methane.

SED
4, 203–239, 2012

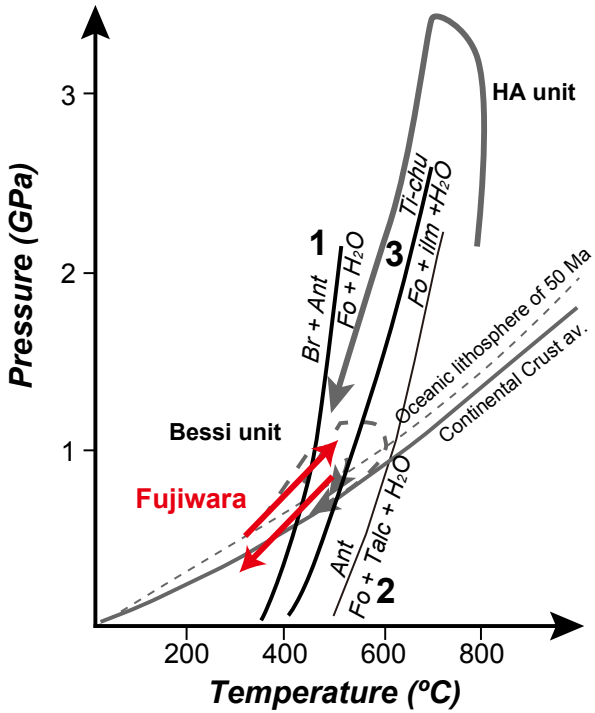

Fig. 9. Possible P-T trajectory for the Fujiwara dunites (red arrows). P-T paths of HA (Higashi-akaishi) and Bessi units and geotherm of continental crust and oceanic lithosphere are also from Mizukami and Wallis (2005) and references therein. Reaction curves 1, 2 and 3 are from Evans (1977), Ulmer and Trommsdorff (1995), and Engi and Lindsley (1980), respectively. The Fujiwara complex was exhumed together with HA and Bessi units after the peak of the Sanbagawa metamorphism, although they were originated from the different depths.

SED
4, 203–239, 2012